Formation of an ordered Si dimer structure on HfB$_2$(0001)

Rasdip Singh and Michael Trenary

Department of Chemistry, University of Illinois at Chicago, 845 West Taylor Street, Chicago, Illinois 60607-7061

Takaho Tanaka

National Institute for Materials Science, 1-1 Namiki, Tsukuba, Ibaraki 305-0044, Japan

Prasenjit Sen and Inder P. Batra

Department of Physics, University of Illinois at Chicago, 845 West Taylor Street, Chicago, Illinois 60607-7061

An ordered surface structure formed after exposure of the HfB$_2$(0001) surface at 800 °C to SiH$_4$(g) followed by annealing at 900 °C has been characterized experimentally with low-energy electron diffraction, scanning tunneling microscopy, and x-ray photoelectron spectroscopy (XPS). The structure is described by a ($\sqrt{7} \times \sqrt{3}$) lattice with a bonded pair of Si atoms in each overlayer unit cell. An absolute Si coverage estimate of 0.48 monolayer based on XPS also supports this structure. Calculations using psuedopotentials within the framework of density functional theory and a five-layer slab model of the substrate show that the threefold hollow site is energetically favored for isolated Si atoms and that Si atoms at next-nearest-neighbor three fold hollow sites will form dimers with a Si-Si distance of ≈ 2.4 Å.

I. INTRODUCTION

The interface between silicon and other materials is of obvious relevance to many applications in such areas as microelectronics[1] and microelectromechanical systems.[2] As device sizes approach the nanometer length scale, the atomic scale details of the interfaces are of increasing importance. Surface science methods are particularly well suited to establish the properties of the first few atomic layers of the interface formed in the course of thin film growth. Such methods have been extensively used in studies of metal film growth on Si surfaces[3] and to a much more limited extent of the growth of silicon thin films on metal surfaces. Refractory metal compounds, such as nitrides, carbides, and borides, are also used in microelectronics for applications such as thin film resistors and as diffusion barriers between the semiconductor and metallic conductors used for interconnects. As Williams has pointed out in a recent overview of the applications of carbides, nitrides, and borides to electronics, of the three classes, the borides have some distinct advantages.[4] This partly stems from the fact that the borides are stoichiometric compounds with a very narrow composition range, in marked contrast to carbides and nitrides, which are interstitial compounds with a wide range of compositions. Williams notes that this is likely the underlying reason why TiB$_2$ thin films show resistivities that are both remarkably low and close to the single-crystal value, whereas TiC or TiN thin film resistivities are generally both much higher and more dependent on the exact preparation conditions used. The technological uses and properties of boride thin films are reviewed by Mitterer.[5] There are more specific studies of the use of diborides as diffusion barriers[6] that also indicate their potential advantages, although the material most commonly used at present is TaN.

The Si-HfB$_2$ interface is studied here by depositing silicon onto a HfB$_2$(0001) single crystal under ultrahigh vacuum (UHV) conditions through the thermal decomposition of silane, SiH$_4$(g), followed by characterization of the surface structures formed with low-energy electron diffraction (LEED), scanning tunneling microscopy (STM), and x-ray photoelectron spectroscopy (XPS). Surface science methods have been used to study silicon deposition via silane decomposition on Ni(100),[7] Pt(111),[8,9] Pd(100),[10] Pd(110),[11,12] Au(100),[13] and Cu(100).[14] Like most other metal borides, HfB$_2$ is a metal in terms of its high electrical conductivity and yet has ceramiclike properties in that it is extremely hard, but brittle, and has a very high melting point of 3380 °C.[15] It has the AlB$_2$ structure common to many diborides, which can be described by a simple hexagonal lattice with three atoms per unit cell. The structure consists of layers of hexagonal close-packed metal atoms alternating with layers of boron atoms with a geometric structure similar to graphite, although the bonding within the boron layers is quite different from that of graphite.[16–19] More details of the diboride structure are described below. The relatively few surface science studies of HfB$_2$(0001) (Refs. 20 and 21) indicate that the surface is metal terminated and consists of a close-packed layer of Hf atoms. STM images are typical of those of a simple metal and showed the surface to consist of broad and flat Hf terraces separated by steps one unit cell in height (3.5 Å) with an apparent corrugation between Hf atoms of less than 0.1 Å, which was too low to allow individual Hf atoms to be resolved. The chemical reactivity of the HfB$_2$(0001) surface is somewhat less than that of Hf(0001).[22] Given the metal-like properties of HfB$_2$(0001), it might be expected that Si deposition onto this surface would yield results similar to those obtained on elemental metal surfaces. However, there is at least one reason why this might not be the case. Whereas the reaction of many pure metals with silicon is highly exothermic, the silicides are generally less thermodynamically stable than the corresponding nitrides, carbides, or borides.[23] Although a large number

of different hafnium silicide phases are known, $HfSi_2$ is the most silicon-rich phase and has a heat of formation of -54.0 kcal/mol, the highest heat of formation per mole of metal among the hafnium silicides. The heat of formation of HfB_2 is -85.6 kcal/mol. Since the reaction of HfB_2 with Si to form $HfSi_2$ and B is endothermic, the interface between silicon and a refractory compound such as HfB_2 may be fundamentally different from the interfaces between Si and elemental metals. For this reason, past studies of the structures that form when silicon is deposited onto the surfaces of elemental metals may provide little guidance as to the expected properties of the $Si/HfB_2(0001)$ interface.

In this study we focus on a particular surface phase of the $Si/HfB_2(0001)$ system in which an ordered array of Si dimers is characterized with LEED and STM. Under other conditions the surface is dominated by phases that correspond to the formation of hafnium silicides. The STM images indicate that the different phases generally coexist on the surface in varying proportions. A description of these other phases will be presented elsewhere. The experimental observations reported here are complemented by density functional theory calculations that show the threefold hollow site to be the lowest-energy site for a single Si atom and that Si dimer formation is also energetically favored for Si coverages of 0.5 and 0.4 monolayer.

II. EXPERIMENT

The surface analysis system used in this study has been described in detail elsewhere.[24,25] It consists of a stainless steel UHV chamber (base pressure during these studies varied from 6×10^{-11} to 2×10^{-10} torr) equipped with instruments for XPS, LEED, and STM. The XPS system consists of a dual-anode Mg-Al x-ray source and a hemispherical sector electron energy analyzer. The spectrometer binding energy scale was calibrated with the Au $4f_{7/2}$ (83.98 ± 0.02 eV) and Ag $3d_{3/2}$ (374.6± 0.02 eV) peaks, according to the method of Powell.[26] Since HfB_2 is a good metallic electrical conductor, no sample charging problems were expected or observed and a flood gun was not used. The UHV-compatible scanning tunneling microscope has been described in detail elsewhere.[27] Etched tungsten tips were used to obtain the images reported here. The preparation and characterization of the clean $HfB_2(0001)$ surface with XPS, LEED, and STM have been described in detail earlier.[21] Briefly, cleaning consisted of a combination of Ar ion sputtering (typically 500 eV, 10–20 μA, for 1.5 h) followed by annealing to 1900 °C by electron bombarment from behind the crystal. This procedure led to a sharp (1×1) LEED pattern and a few percent of oxygen, the only contaminant observed after cleaning. The $HfB_2(0001)$ crystal was grown at the National Institute for Materials Science in Tsukuba, Japan. It was oriented with Laue back reflection to within 1° of the (0001) plane, cut by spark erosion, and polished to a mirror finish with boron carbide powder followed with diamond-based polishing compounds. Silicon deposition was achieved through exposure of the sample held at 800 °C to pure silane. This was followed by annealing to 900 °C. These particular conditions were chosen to achieve measur-
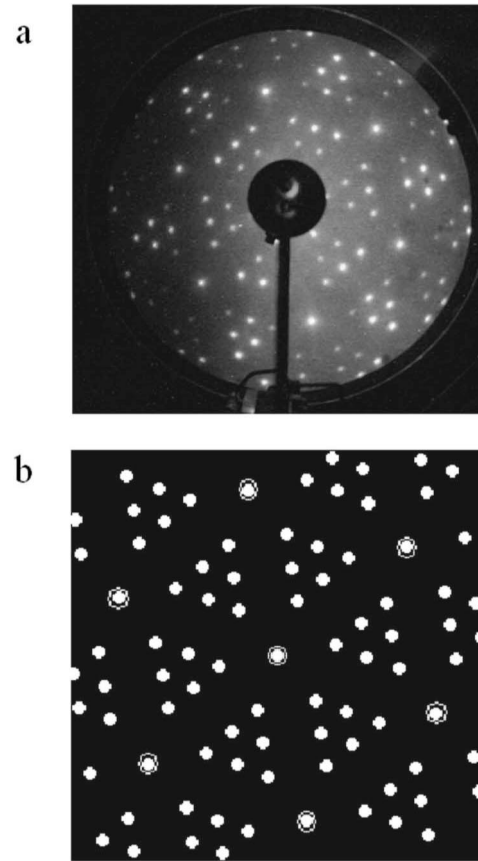

FIG. 1. (a) Observed LEED pattern of the $Si/HfB_2(0001)$ dimer structure at 118.0 eV and (b) LEED pattern predicted for a ($\sqrt{7} \times \sqrt{3}$) structure.

able quantities of silicon as determined by XPS and well-ordered structures as determined by LEED and STM. Since pure $SiH_4(g)$ reacts explosively with air and water, special precautions are needed to handle it safely. We placed a stainless steel rod heated to 850 °C in the pumping manifold between the turbopump and the backing mechanical pump. The silane decomposes on the heated rod to produce $Si(s)$ and $H_2(g)$, thereby preventing formation of SiO_2 in the mechanical pump, which could lead to pump damage. The silane exposure was through a doser placed about 2.5 cm from the sample. Exposures are based on background chamber pressure, which rose to 7×10^{-9} torr during dosing and, therefore, underestimate the true exposures at the sample.

III. COMPUTATIONAL METHOD

First-principles calculations are carried out using the pseudopotential method within density functional theory (DFT). We studied bulk HfB_2, $HfB_2(0001)$, and Si-covered-$HfB_2(0001)$ surfaces. Our bulk system consisted of a unit cell containing one Hf and two B atoms in the AlB_2-type hexagonal structure [Fig. 2(b)]. The $HfB_2(0001)$ surface is represented in the repeated slab supercell geometry. Each slab contains a total of five layers: three Hf and two B layers representing a Hf-terminated surface. Further, each Hf layer contains 4 atoms and each B layer contains 8 atoms for a
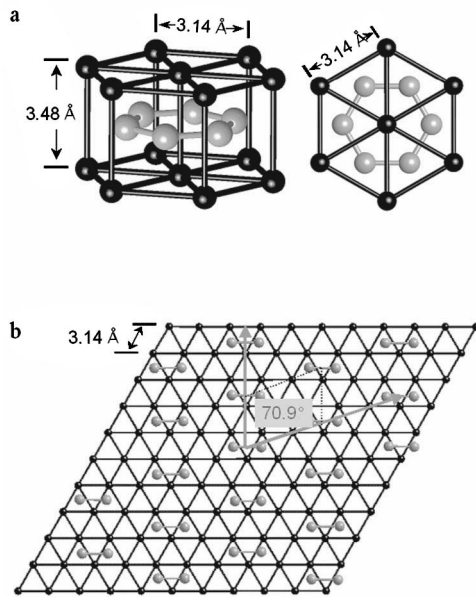
FIG. 2. (a) Perspective view and view along the *c* axis of the bulk HfB$_2$ structure. (b) Proposed dimer structure based on LEED and STM observations supported by DFT calculations.

total of 28 atoms in the supercell. The top three atomic layers, i.e., the top two Hf layers and one B layer, are relaxed for geometry optimization while the bottom two layers are held fixed to simulate a bulklike termination. We include a 9 Å vacuum space between two successive slabs. All the wave functions are expanded in a plane-wave basis set with a cutoff energy of $|\mathbf{k}+\mathbf{G}|^2 \leqslant 300$ eV. The Brillouin-zone (BZ) integration is performed within the Monkhorst-Pack scheme.[28] We use an $(8\times8\times8)$ **k** mesh for the bulk calculation and an $(8\times8\times1)$ **k** mesh for the surface calculations. This fine mesh is required for a metallic system. Convergence with respect to energy and the number of **k** points was tested. Ionic potentials are represented by Vanderbilt-type ultrasoft pseudopotentials[29] and the results are obtained within the generalized gradient approximation (GGA) (Ref. 30) for fully relaxed atomic structures. A preconditioned conjugate gradient is used for wave function optimization and a conjugate gradient method for ionic relaxations. The *z* axis is taken perpendicular to the (0001) surface while *x* and *y* axes are in the plane. All our calculations are performed using the VASP code.[31]

IV. EXPERIMENTAL RESULTS

The HfB$_2$ crystal was exposed to various amounts of silane at a variety of temperatures. At room temperature, silane was found to dissociate on the clean surface, most likely forming various silicon hydrides, atomic hydrogen, and adsorbed silicon atoms. No ordered structures were observed with LEED or STM. This observation is in agreement with low-temperature silane chemistry, where coadsorbed hydrogen has been found to significantly degrade surface order as observed in Si molecular beam epitaxy on Si (111)-(1 ×1):H (Refs. 32 and 33) and during chemical vapor deposition (CVD) of disilane.[34] At higher temperatures (>800 °C), various hafnium silicides and silicon dimers were observed. The silicides were found to dominate the surface at lower exposures [<60 L (1 L=10^{-6} torr sec)], while silicon dimers were found to dominate the surface at higher exposures (>60 L).

Figure 1(a) shows a LEED pattern observed after a nominal 60 L exposure to silane with the sample at 800 °C followed by a 900 °C anneal. Figure 1(b) shows the simulated LEED pattern[35] based on a lattice that can be represented in matrix notation as

$$\begin{pmatrix} 2 & 1 \\ -1 & 2 \end{pmatrix}.$$

The simulation assumes three equivalent domains rotated by 120°. There is clearly excellent agreement between the observed and simulated patterns indicating no ambiguity regarding the long-range order of the Si overlayer. The edges of the superstructure unit cell have lengths of $\sqrt{7}$ and $\sqrt{3}$ relative to the substrate unit cell, or 8.31 Å and 5.44 Å, based on a substrate lattice constant of 3.14 Å. The bulk structure of HfB$_2$ is illustrated in Fig. 2(a) and a real space model of the $(\sqrt{7}\times\sqrt{3})$ Si dimer structure relative to the topmost atomic layer of the substrate, which consists of the Hf atoms shown in black, is shown in Fig. 2(b). The gray dumbbells represent the silicon dimers. The structural model combines information from the STM images, the LEED pattern, and the DFT calculations described below, which indicate that the silicon atoms of the dimers are not located exactly in the middle of the threefold hollow sites but are shifted by 0.40 Å towards each other. This shift is included in the model shown in Fig. 2(b).

Figure 3 shows two STM images of the surface corresponding to the LEED pattern of Fig. 1. Figure 3(a) reveals two domains rotated with respect to each other by 120°, a boundary between two domains of the same azimuthal orientation that appears as a dark jagged line, and structure attributed to a silicide. The identification of silicides is based on correlations between structures observed with STM and chemical shifts of the Si 2*p* peak as observed with XPS. The ordered array of the oblong objects are shown in more detail in the close-up image of Fig. 3(b), where the objects are seen to be oriented perpendicular to the row directions. Based on the arguments presented below, these objects are identified as Si dimers. The unit cell associated with the dimers has one vector 5.4 Å long oriented parallel to the rows and a second vector at an angle of 76°±1° from the first with a length of 8.3 Å. Although the difference in angle between the unit cell vectors seen with STM (76°) and deduced from LEED (71°) is small, it appears to be greater than the precision of the measurement from the STM images. It is not clear if the difference is due to inaccuracies in the measurement or to a real effect. The dimers have an average length of ~4 Å. Thus, not only does the two-dimensional (2D) periodicity seen in the STM image agree with that of the LEED pattern, but also the length and orientation of the objects in the STM image are consistent with the unit cell containing Si dimers as shown in Fig. 2(b). The proposed dimer-row structure
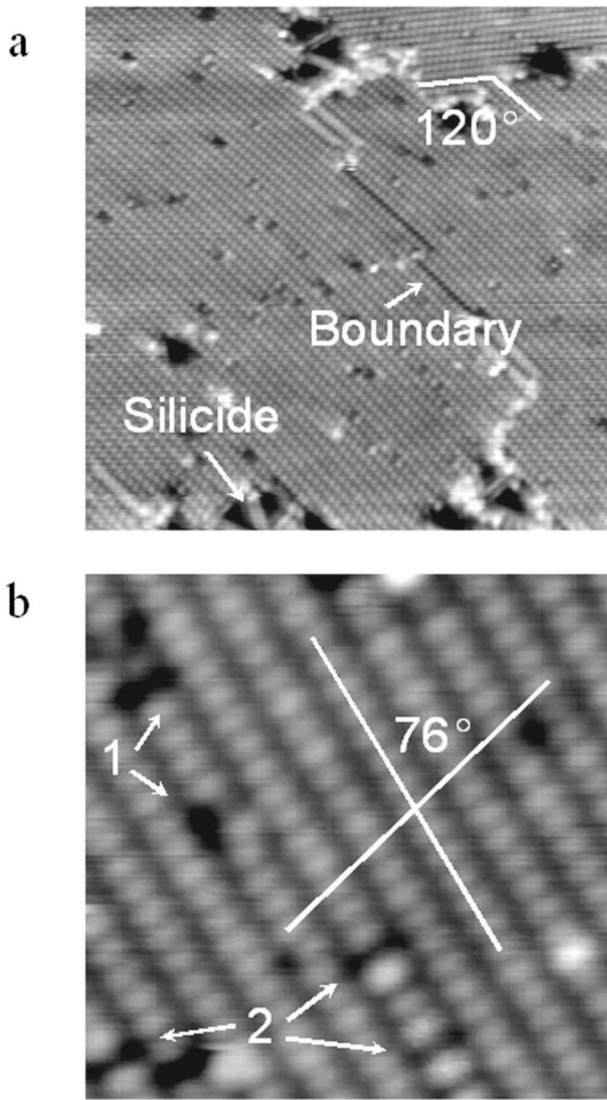
FIG. 3. Constant-current STM images of the $Si/HfB_2(0001)$ dimer structure. (a) 397×397 Å^2, sample bias $+1.5$ V, 0.7 nA. A rotational domain oriented 120° from the main dimer-row domain is seen in the upper right. A domain boundary within the main dimer-row domain appears as a jagged dark line in the middle of the image. At the lower left is structure associated with silicide formation. (b) 85×85 Å^2 at sample bias of $+1.5$ V, 1.0 nA. Lines are drawn along the two lattice vectors of the dimer-row structure showing that there is an apparent angle of 76° between the two directions. The arrows point to the two types of dark spots that are described in the text.

bears some resemblance to the dimer-row structure seen on the Si(100)-2×1 surface, where the Si-Si distance is 2.38 ± 0.04 Å, a value close to that of bulk Si, 2.35 Å.[36] However, the structure seen here is distinctly different in that it is described by a 5.4×8.3 Å^2 nonrectangular unit cell as opposed to the 3.84×7.68 Å^2 rectangular unit cell of Si(100)-2×1.

Two different kinds of dark spots, labeled features 1 and 2, are apparent in Fig. 3(b). Feature 1 appears to interact with the dimers, causing them to be displaced slightly from their normal positions. Because the size and shape of the dis-

placed dimers are identical to dimers in unperturbed areas, feature 1 cannot simply be silicon atom vacancies. Also, these dark spots are seen to be centered between dimers, which according to the structural model of Fig. 2(b) would place them above unoccupied threefold hollow sites. These dark features are found to aggregate along and in between dimer rows as well as across rows. The origin or identity of these features is not known at present. Feature 2 is always found to be symmetric on both sides of the dimer rows and to decrease in intensity across the row. These are believed to be silicon dimer vacancies and are very similar to silicon dimer vacancies on Si (100)-(2×1). Under the conditions of this STM image, single silicon atoms were not observed. This result implies that single Si atoms are not stable on the surface under these conditions, in agreement with the DFT calculation.

If the dimer structure of Fig. 2(b) covered the whole surface, it would correspond to a Si coverage of 0.40, i.e., the ratio of Si atoms to Hf atoms in the topmost layer of the substrate. In fact, although the LEED pattern of Fig. 1 suggests that large areas of the surface are covered by the ($\sqrt{7}\times\sqrt{3}$) structure, STM images show that this structure invariably coexists with more complex phases. Under the conditions used for Figs. 1 and 3, the ($\sqrt{7}\times\sqrt{3}$) structure appears to cover no more than 80% of the surface. As an independent measure of the Si coverage, XPS spectra were obtained following silane exposures at 800 °C and annealing to 900 °C. Following this treatment, the Si $2p$ peak has an area that is 37% of the B $1s$ peak area and 16% of the Hf $4f_{7/2}$ area, a result consistent with a coverage in the submonolayer range. The use of appropriate sensitivity factors[37] yields a Si:Hf ratio of 0.48 ± 0.05, where error bars reflect the uncertainty in measuring the Si $2p$ peak area. Although the LEED and STM results are also suggestive of a submonolayer Si coverage, the independent quantitive estimate of the coverage by XPS is important since, given the lack of knowledge of the dissociative sticking probability of SiH_4 on the $HfB_2(0001)$ surface, a nominal 60 L exposure could conceivably result in the deposition of multilayers of Si. The coverages obtained for various exposures indicate a sticking probability of less than 1×10^{-2}, which decreases with increasing coverage. A sticking probability of this magnitude is consistent with previous studies in which silane was used to deposit silicon onto metal surfaces.[7]

V. COMPUTATIONAL RESULTS

A. Bulk system

The bulk system is based on the three-atom unit cell illustrated in Fig. 2(a), which is initially assumed to have the indicated experimentally determined[38] lattice constants. This structure is then relaxed to optimize the shape and size of the cell and the positions of the atoms within the cell. The in-plane lattice constant changes slightly to give $a=3.13$ Å and the c-lattice constant remains unchanged at 3.48 Å. These numbers are in good agreement with experiment and are comparable to the results of an earlier calculation.[19] The cohesive energy of the bulk HfB_2 is found to be 26.45 eV per HfB_2 primitive cell.
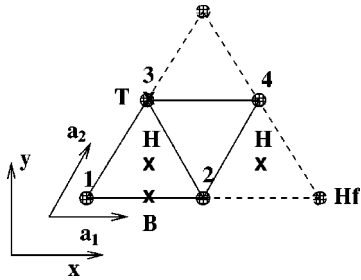
FIG. 4. The (2×2) surface unit cell with four Hf atoms. The periodic images of atom 1 along the lattice vectors $\mathbf{a_1}$ and $\mathbf{a_2}$ are shown by dotted lines. The three special symmetry points on the surface are labeled **H** (hollow), **B** (bridge), and **T** (top).

B. Clean HfB$_2$(0001) surface

For the surface calculation, we employ the repeated slab geometry with each slab containing five layers—three Hf and two B layers. Based on previous theoretical and experimental studies,[19–21] we treat HfB$_2$(0001) as a Hf-terminated surface. The in-plane lattice constant and the layer separation are set equal to the values obtained in our bulk calculation. Important questions in a surface calculation are the possible surface reconstructions and the change in interlayer separations. We do not find any reconstruction of the Hf-terminated surface. The Hf atoms experience almost no force at their bulk terminated positions and the in-plane lattice constant remains unchanged. However, the interlayer separations show some changes. The first interlayer separation decreases by 3.4%. The second interlayer separation increases by 0.4%. Yamamoto *et al.*[19] found the changes in the first and second interlayer separations to be -4.8% and $+0.89\%$, respectively, for HfB$_2$(0001). This behavior of the first two interlayer separations is opposite to that of a B-terminated TaB$_2$(0001) surface and has been understood in terms of the amount of charge transferred from the metal d orbitals to the boron p orbitals.[19]

C. Si-covered-HfB$_2$(0001) surface

It is important to compare the relative energetics of Si adsorption at various symmetry sites before examining the surface structure at higher coverages. We employ a (2×2) surface unit cell on which a Si atom is placed at three special symmetry sites on the unreconstructed Hf-terminated surface. We calculate the binding energy of Si at the threefold hollow (**H**), twofold bridge (**B**), and on-top (**T**) sites. These sites are labeled in Fig. 4. The **H** site turns out to be energetically the most favorable one for a Si atom with a binding energy $E_b^H=5.91$ eV. This is followed by the **B** and **T** sites with $E_b^B=5.56$ eV and $E_b^T=4.74$ eV, respectively. This sequence of binding energies is qualitatively consistent with the intuitive chemical expectation that the hollow site should be favored because it has a higher coordination than the other two sites. The distances of the Si adatom from the different surface Hf atoms are listed in Table I.

We are now in a position to understand the structure of the Si covered HfB$_2$(0001) surface at higher coverages. First we consider a Si coverage of 0.5 monolayer (ML) which is

TABLE I. The distances of a single Si adatom, located at various symmetry points, from the different surface Hf atoms and its height above the Hf plane.

Si position	Distance (in Å) from			Height (Å)
	Hf(1)	Hf(2)	Hf(3)	
H	2.65	2.65	2.65	1.91
B	2.59	2.59	3.31	1.96
T	3.96	3.96	2.56	2.40

easier to deal with computationally than the experimentally determined coverage of 0.4 ML. At 0.5 ML, we have two Si adatoms for the four surface Hf atoms. Since the **H** site is the energetically most favorable one, we put the two Si atoms at the two **H** sites in our (2×2) supercell (Fig. 4). On relaxing the system, the Si atoms experience no forces along the x direction. They move down marginally (~0.1 Å) along the $-y$ direction. Their interatomic distance remains unchanged at 3.13 Å. The binding energy per Si adatom in this configuration is found to be 5.75 eV. This suggests that the presence of the first Si adatom at one of the **H** sites, with a binding energy of 5.91 eV, decreases the binding energy of the second Si adatom. From the large Si-Si distance of 3.13 Å, it is clear that the Si adatoms at the **H** sites are not dimerized. This is further confirmed by the charge density contour plot in the plane of the Si atoms shown in Fig. 5(a).

In order to assess the dimer model suggested by the experiments, we moved the Si atoms on the **H** sites closer to each other along x, so that they are 2.30 Å apart. Upon relaxing this structure, we find that they experience a small
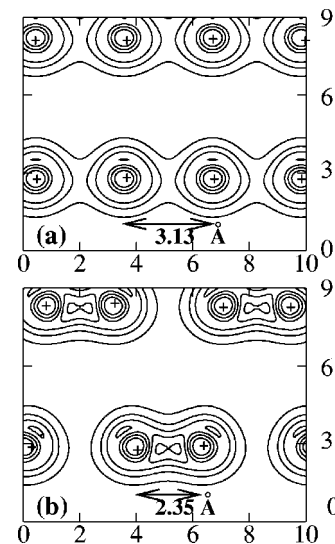

FIG. 5. Charge density contour plots in the plane of the adatoms for 0.5 ML Si on the HfB$_2$(0001) surface. (a) Si atoms are not dimerized as can be seen from the very small charge density between two adjacent Si atoms. (b) Si atoms are dimerized with maximum charge density occurring between them. Positions of the Si atoms are marked.

TABLE II. Distances of the two Si adatoms from the surface Hf atoms at 0.5 ML are given both for the undimerized and the dimerized structures. Heights of the Si planes above the Hf plane are also listed.

Si position	Distance (in Å) from				Height (Å)
	Hf(1)	Hf(2)	Hf(3)	Hf(4)	
		Undimerized			
Si(1)	2.73	2.73	2.82	–	
					2.05
Si(2)	–	2.73	–	2.82	
		Dimerized			
Si(1)	2.91	2.64	2.77	–	
					1.97
Si(2)	–	2.64	–	2.77	

TABLE III. Distances of the two Si adatoms from the surrounding four Hf substrate atoms and the height of the Si plane above the Hf layer at 0.4 ML in the optimum dimerized geometry.

Si position	Distance (in Å) from				Height(Å)
	Hf(1)	Hf(2)	Hf(3)	Hf(4)	
Si(1)	2.86	2.64	2.82	–	
					2.01
Si(2)	–	2.64	–	2.81	

repulsive force along x and, in the optimized structure, are 2.35 Å apart and 1.97 Å above the Hf layer. This separation between the two Si atoms, being close to their bulk separation, suggests that they form a dimer bond. We show a charge density contour plot for this configuration in the plane of the Si atoms in Fig. 5(b). The bond between the Si atoms is clearly seen. The binding energy in this configuration is 5.93 eV per Si adatom, which is greater by 0.18 eV than for the undimerized case. This energy is much less than that of a normal Si-Si bond (≈ 1 eV) because dimerization occurs at the expense of a weakened Si-Hf interaction. The results imply that there must be an energy barrier separating the undimerized structure in which the two Si atoms are at the **H** sites with a separation of 3.13 Å and the dimerized one with a Si-Si distance of 2.35 Å. Otherwise the former structure would have readily relaxed into the latter one upon geometry optimization. The Si-Hf bond lengths for both the dimerized and undimerized structures are shown in Table II.

The calculations described above correspond to a Si coverage of 0.5 ML whereas the LEED pattern implies an ideal coverage of 0.4 ML. For a more exact correspondence between theory and experiment, we also did a calculation at 0.4 ML. This requires a bigger surface unit cell as the number of surface Hf atoms has to increase for each Si pair. Moreover, the symmetry of the system is now very different from what it is at 0.5 ML. The surface unit cell of the system at 0.4 ML Si coverage is exactly as shown by the dotted line in Fig. 2(b). The two lattice vectors in the plane are 8.31 Å and 5.43 Å, making an angle of 70.9° with each other. This system contains 5 Hf atoms in each Hf plane and hence 10 B atoms in each B plane. Having 3 Hf and 2 B layers as before, the system now has 15 Hf, 20 B, and 2 Si atoms. Starting from a configuration in which the Si atoms are exactly at the hollow sites, they spontaneously move closer on relaxation and are 2.4 Å apart in the optimum geometry. The Si adatoms are 2.01 Å above the Hf layer, very similar to the value at 0.5 ML. The distances of the two Si adatoms from the closest Hf atoms are given in Table III. A Si-Si distance of 2.4 Å suggests that they readily dimerize at this coverage without the barrier found at 0.5 ML. The dimerization is confirmed by the charge density in the plane of the Si adatoms as shown in Fig. 6.

The most obvious difference between the STM images of the clean and Si covered HfB_2(0001) terraces is that the latter reveals well-resolved structure, whereas the former appears flat and featureless. A qualitative understanding of this difference is provided by plots of the charge densities for the two cases. The STM tip scans the surfaces from some height, depending on the bias voltage and current. To mimic this, we show charge densities in planes 2 Å above the surface for both the clean and 0.5 ML Si covered surfaces in Fig. 7. This figure shows that on the clean Hf-terminated surface, because of the metallic nature of the bonding, there is very little corrugation of the charge density and hence the STM image looks quite uniform. On the other hand, in the presence of the Si adatoms, there is a larger variation in the charge density. But the dip in the charge density halfway between the two Si atoms of a dimer is quite small compared to the overall scale of the variation. This is why we see extended bright patches where the dimers are located and cannot resolve the individual Si atoms in them.

VI. DISCUSSION

The silicon dimer structure on HfB_2(0001) proposed here fully incorporates the complementary information provided by the experimental techniques of LEED, STM, and XPS as well as by the information obtained from first-principles electronic structure calculations based on DFT. The observed LEED pattern reveals that the structure possesses good long-range order with statistically distributed rotationally equivalent domains. Since the pattern corresponds to a single phase,
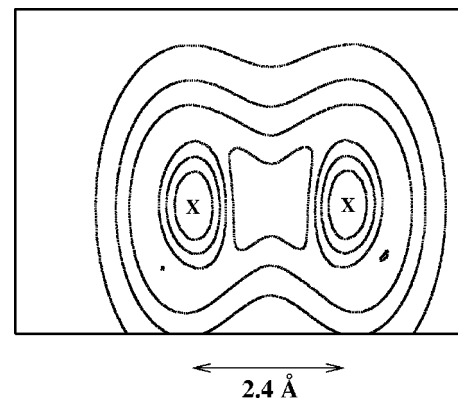

FIG. 6. Charge density contour plot in the plane of the adatoms for 0.4 ML Si on the HfB_2(0001) surface with a Si-Si distance of 2.4 Å showing dimer formation.
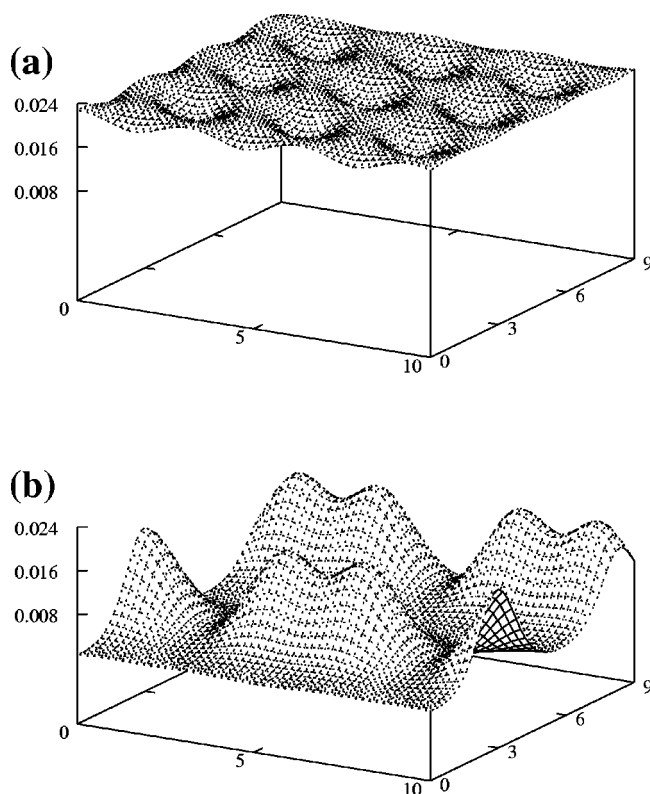
FIG. 7. Surface plots for charge densities in planes 2 Å above the (a) clean $HfB_2(0001)$ surface (there is very little charge corrugation in the plane, as expected for metallic bonding) and (b) Si dimers on the $HfB_2(0001)$ surface. The magnitude of the charge density corrugation is much larger compared to (a), which makes the Si dimers easily identifiable with STM.

it indicates that this phase is dominant on the surface under the conditions used. While the STM images reveal the same periodicity as implied by LEED, the latter results establish that the structure observed with STM is representative of the entire surface. However, the LEED pattern does not provide any information on the content of the unit cell whereas the STM images of rows of oblong objects strongly suggest that the structure is not simply due to an ordered array of isolated adsorbed Si atoms. The relationship between the dimer orientation and the two-dimensional lattice vectors revealed in the STM images is strongly supportive of the structure proposed. The XPS results are also supportive of this structure in that they imply a submonolayer coverage close to the value implied by the proposed structure. The experimental results do not reveal the placement of the Si atoms on the substrate sites. This is because not only are Hf atoms not visible in the $Si/HfB_2(0001)$ case, but they are not resolved even for the clean surface. The DFT calculations showing

that the threefold hollow site is favored for isolated Si atoms and that two Si atoms at neighboring threefold hollow sites can form a bond provides the necessary additional information to establish the complete structure. The formation of the Si-Si bond explains the row structure and even the size of the oblong objects, which are not necessarily established to be dimers from the STM images alone. The dimer-row structure seen here bears resemblance to the structure seen on the $Si(100)$-2×1 surface. In that case, both symmetric and buckled dimers are seen with STM and the relative stability of the two has been the subject of much study.[39] In the present case, the placement of the two Si atoms at equivalent threefold hollow sites predicts a symmetric dimer, consistent with the STM images. The fact that the dimers are symmetric indicates that the energy gained by forming the Si-Si bond with a distance close to the value in bulk Si is not offset by the cost in energy of displacing the Si atoms from the position at the center of the threefold hollow and that this cost is lower than would be involved in leaving one Si atom of the pair in the center of the threefold hollow and displacing the other Si atom towards the first. Such a scenario would result in an inequivalency between the two atoms of the dimer, which would likely be apparent in the STM image, contrary to what is observed.

A key issue in considering the interface between Si and other materials is whether a reaction takes place to form silicides. The structures observed in previous studies following high-temperature processing of either Si deposited onto elemental metal surfaces or through metal deposition onto silicon surfaces are invariably attributed to silicide formation. However, the structure illustrated in Fig. 2(b) is more akin to simple adsorption onto the unreconstructed sites of the substrate surface. To be sure, under other conditions we do observe more complex structures in the $Si/HfB_2(0001)$ system that we attribute to hafnium silicides. But it may well be the case that the dimer row structure reported can form only because of the high thermodynamic stability of HfB_2 relative to $HfSi_2$, which allows unique structures to form at the Si/HfB_2 interface that cannot form at simple metal-Si interfaces. This may explain why the borides and other refractory metal compounds have been found to be preferable to simple metals for applications in microelectronics and suggests that they may serve as substrates for the growth of novel structures that cannot be formed on elemental metal surfaces.

[1] C. R. M. Grovener, *Microelectronic Materials* (Institute of Physics Publishing, Bristol, 1989).

[2] K.E. Peterson, Proc. IEEE **70**, 420 (1982).

[3] V. G. Lifshits, A. A. Saranin, and A. V. Zotov, *Surface Phases on*

Silicon: Preparation, Structures, and Properties (Wiley, New York, 1994).

[4] W.S. Williams, JOM **49**, 38 (1997).

[5] C. Mitterer, J. Solid State Chem. **133**, 279 (1997).

[6] J.R. Shappirio, J.J. Finnegan, and R.A. Lux, J. Vac. Sci. Technol. B **4**, 1409 (1986).

[7] L.H. Dubois and B.R. Zegarski, Surf. Sci. **204**, 113 (1988).

[8] J.C. Bondos, A.A. Gewirth, and R.G. Nuzzo, J. Phys. Chem. B **103**, 3099 (1999).

[9] U. Diebold, L.P. Zhang, J.F. Anderson, and P. Mrozek, J. Vac. Sci. Technol. A **14**, 1679 (1996).

[10] C.J. Ennis, D.J. Spence, S.P. Tear, and E.M. McCash, Phys. Rev. B **61**, 8443 (2000).

[11] N. Wälchli, E. Kampshoff, and K. Kern, Surf. Sci. **368**, 258 (1996).

[12] N. Wälchli, E. Kampshoff, A. Menck, and K. Kern, Surf. Sci. **382**, L705 (1997).

[13] J. Han, D. Jeon, and Y. Kuk, Surf. Sci. **376**, 237 (1997).

[14] A.P. Graham, B.J. Hinch, G.P. Kochanski, E.M. McCash, and W. Allison, Phys. Rev. B **50**, 15 304 (1994).

[15] *Binary Alloy Phase Diagrams*, 2nd ed., edited by T. B. Massalski (ASM, Metals Park, OH, 1990).

[16] A.C. Switendick, in *Boron-Rich Solids*, edited by D. Emin, T.L. Aselage, A.C. Switendick, B. Morosin, and C.L. Beckel, AIP Conf. Proc. No. 231 (AIP, NY, 1991), p. 54.

[17] X.B. Wang, D.C. Tian, and L.L. Wang, J. Phys.: Condens. Matter **6**, 10 185 (1994).

[18] K. Lie, R. Høier, and R. Brydson, Phys. Rev. B **61**, 1786 (2000).

[19] K. Yamamoto, K. Kobayashi, H. Kawanowa, and R. Souda, Phys. Rev. B **60**, 15 617 (1999).

[20] W. Hayami, R. Souda, T. Aizawa, and T. Tanaka, Surf. Sci. **415**, 433 (1998).

[21] C.L. Perkins, R. Singh, M. Trenary, T. Tanaka, and Yu. Paderno, Surf. Sci. **470**, 215 (2001).

[22] M. Belyansky and M. Trenary, Inorg. Chim. Acta **289**, 191 (1999).

[23] G. V. Samsonov and I. M. Vinitskii, *Handbook of Refractory Compounds* (Plenum, New York, 1980).

[24] W.C. Foo, J.S. Ozcomert, and M. Trenary, Surf. Sci. **255**, 245 (1991).

[25] J.S. Ozcomert, Ph.D. thesis, University of Illinois at Chicago, 1992.

[26] C.J. Powell, Surf. Interface Anal. **23**, 121 (1995).

[27] J.S. Ozcomert and M. Trenary, J. Vac. Sci. Technol. A **10**, 2581 (1992).

[28] H.J. Monkhorst and J.D. Pack, Phys. Rev. B **13**, 5188 (1976).

[29] D. Vanderbilt, Phys. Rev. B **41**, 7892 (1990); G. Kresse and J. Hafner, J. Phys.: Condens. Matter **6**, 8245 (1994).

[30] J.P. Perdew, J.A. Chevary, S.H. Vosko, K.A. Jackson, M.R. Pederson, D.J. Singh, and C. Fiolhais, Phys. Rev. B **46**, 6671 (1992).

[31] G. Kresse and J. Hafner, Phys. Rev. B **47**, R558 (1993); G. Kresse and J. Furthmüller *ibid.* **54**, 11 169 (1996).

[32] M. Copel and R.M. Tromp, Surf. Sci. **337**, L773 (1995).

[33] M. Horn-von Hoegen and A. Golla, Surf. Sci. **337**, L777 (1995).

[34] U. Kohler, L. Andersohn, and B. Dahlheimer, Appl. Phys. A: Solids Surf. **57**, 491 (1993).

[35] The LEEDPAT program was written by K. Hermann and M. A. Van Hove and is available at http://w3.rz-berlin.mpg.de/~hermann/LEEDpat/.

[36] Average and standard deviation of four independent determinations as compiled in P. R. Watson, M. A. Van Hove, and K. Hermann, J. Phys. Chem. Ref. Data, Monograph No. 5, 1994, pp. 725-732 (1994).

[37] J.H. Scofield, J. Exp. Theor. Phys. **8**, 129 (1976).

[38] R. W. G. Wyckoff, *Crystal Structures* (Interscience, New York, 1965), Vol. 1.

[39] J. Dąbrowski and H.-J. Müller, *Silicon Surfaces and Formation of Interfaces* (World Scientific, Singapore, 2000).